Available online at www.sciencedirect.com
ScienceDirect
Trans. Nonferrous Met. Soc. China 30(2020) 405−416
Transactions of Nonferrous Metals Society of China
www.tnmsc.cn

Effect of strain rate difference between inside and outside groove in M−K model on prediction of forming limit curve of Ti6Al4V at elevated temperatures

Xiao-qiang LI[1], Hong-rui DONG[1], Hai-bo WANG[2], Gui-qiang GUO[1], Dong-sheng LI[1]

1. School of Mechanical Engineering and Automation, Beihang University, Beijing 100191, China;
2. School of Mechanical and Materials Engineering, North China University of Technology, Beijing 100144, China

Received 4 April 2019; accepted 5 December 2019

Abstract: The influence of initial groove angle on strain rate inside and outside groove of Ti6Al4V alloy was investigated. Based on the evolution of strain rate inside and outside groove, the effect of strain rate difference on the evolution of normal stress and effective stress inside and outside groove was also analyzed. The results show that when linear loading path changes from uniaxial tension to equi-biaxial tension, the initial groove angle plays a weaker role in the evolution of strain rate in the M−K model. Due to the constraint of force equilibrium between inside and outside groove, the strain rate difference makes the normal stress inside groove firstly decrease and then increase during calculation, which makes the prediction algorithm of forming limit convergent at elevated temperature. The decrease of normal stress inside groove is mainly caused by high temperature softening effect and the rotation of groove, while the increase of normal stress inside groove is mainly due to strain rate hardening effect.
Key words: Ti6Al4V alloy; strain rate difference; forming limit; M−K model; stress evolution

1 Introduction

The forming limit curve (FLC) is widely adopted to characterize the formability of sheet metals during plastic forming processes [1,2]. However, the determination of FLC using experimental method is hard to achieve, due to the extreme high requirement on multiple tests and complicated loading paths. Therefore, it is more attractive to obtain FLC through theoretical prediction. M−K model, a mathematical model proposed by MARCINIAK and KUCZYŃSKI [3] in 1967, has been widely used for the FLC prediction because of its practicability and simplicity [4]. M−K model assumes a groove to characterize original imperfection of sheet metal, which leads to the difference of strain between inside and outside groove, as shown in Fig. 1 [3]. Necking occurs when the ratio of strain increment between inside and outside groove is larger than a certain value. Generally, the area outside groove is marked as Area *a* and the area inside groove is marked as Area *b*.

With increasing requirement for lightweight in automotive and aerospace industries, many high-performance materials become more and more popular, such as magnesium alloy, titanium alloy and ultrahigh strength aluminum alloy. However, their formability at room temperature is poor, which largely limits their applications. Research shows that increasing forming temperature is an effective way to improve their formability [5,6]. Therefore, the study on their formability and the FLC prediction at elevated temperatures attract much attention.

Foundation item: Project (51775023) supported by the National Natural Science Foundation of China; Project (YWF-18-BJ-J-75) supported by the Fundamental Research Funds for the Central Universities, China
Corresponding author: Xiao-qiang LI; Tel: +86-13810937753; E-mail: lixiaoqiang@buaa.edu.cn
DOI: 10.1016/S1003-6326(20)65222-0

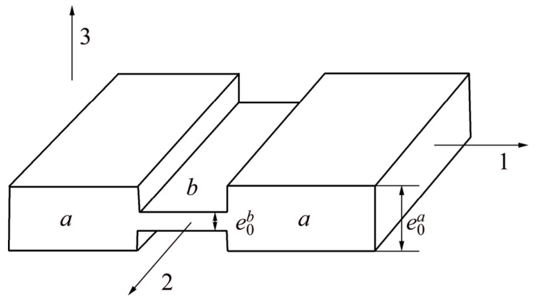

Fig. 1 Diagram of original M−K model [3]

The effects of yield criterion and constitutive model on the theoretical FLC prediction have been widely studied by many researchers. WU et al [7] investigated the effect of yield criterion on theoretical FLC prediction of Ti22Al24.5Nb0.5Mo sheet at 1243 K. It was shown that Logan–Hosford yield function was more appropriate than von Mises or Hill48 yield function. By introducing Backofen constitutive model into M−K theory, CAO et al [8] studied the effects of different yield criteria on the theoretical FLC prediction of AZ31 at 473 and 523 K and concluded that Hill48 yield criterion was more appropriate than von Mises yield criterion for warm forming. According to continuum damage mechanics, ZHOU et al [9] formulated some damage-coupled constitutive models to predict the FLC of 22MnB5 at elevated temperatures. The result showed that the predicted FLC agreed well with corresponding experimental results. Based on Backofen constitutive model, Hosford yield criterion and M−K theory, the effect of stress exponent of yield criterion on the FLC prediction of Al5083-O was investigated by HOU et al [10]. It was found that the established prediction model was appropriate and better prediction results could be obtained when stress exponent M was 6. KOTKUNDE et al [11] investigated the effect of yield model on FLC of Ti6Al4V in warm condition. The results showed that Hill yield model and Barlat yield model were the most suitable models for FLC prediction in the right side and left side regions, respectively. Hence, it is reasonable to conclude from current literatures that for the accurate FLC prediction, it is important to choose appropriate yield criterion and constitutive model for different materials.

Based on established FLC prediction model, the effect of process parameters on forming limit has been studied. By introducing von Mises yield criterion into M−K model, the influences of strain rate and temperature on FLC of Ti6Al4V alloy were investigated [12]. It was found that increasing temperature and decreasing strain rate could enhance FLC level, which has also been observed by MIRFALAH-NASIRI et al [13], SHAO et al [14] and LI et al [15]. By combining M−K model with a crystal plasticity model, NEIL and AGNEW [16] investigated the effect of temperature on FLC of AZ31B. It was found that the anisotropy of strain and strength decreased with the increase of temperature. By incorporating Logan−Hosford yield function into M−K model, CHAN and LU [17] studied the effect of material sensitivity on FLC of AZ31B at elevated temperature with verified prediction model. It was shown that the effect of strain rate became more obvious with the increase of temperature, which was the same as the study of ZHENG and CHEN [18]. GAO et al [19] studied the theoretical FLC prediction of AA2060 with different loading paths during hot stamping process, and showed that the maximum thinning region did not necessarily cause the occurrence of necking and the ratio of incremental work per unit volume could determine the FLC of AA2060. LIU et al [20] investigated the effects of thickness imperfection coefficient and temperature on FLC of ZK60 magnesium alloy sheet. It was shown that the increase of temperature and thickness imperfection coefficient had a positive effect on the improvement of forming limit. MA et al [21] took temperature history into account during the FLC prediction. The result demonstrated that temperature history could improve forming limit. In summary, higher FLC of materials with poor formability can be obtained by adopting high forming temperature. Moreover, the FLC prediction is more sensitive to strain rate at elevated temperatures than that at room temperature.

Overall, regarding to material models, the predicted FLC is mainly affected by yield criterion and constitutive model. While in respect of process parameters, the predicted FLC at elevated temperature is mainly affected by the interaction of strain rate and temperature. It is worth noting that the existing researches focused on the deformation rate of sheet metal. However, in M−K model, the strain rate inside groove is larger than that outside groove. Moreover, strain rate difference will become more apparent during deformation. As titanium alloy generally has high strain rate sensitivity at elevated temperatures, it is necessary to investigate the effect of evolution of strain rate and corresponding stress on the FLC prediction at elevated temperatures.

In this work, the Grosman equation was fitted to characterize the flow behavior of Ti6Al4V by referring to the data in Ref. [12]. Based on the fitted Grosman equation, the prediction model of FLC was established by incorporating the von Mises yield criterion into modified M−K model. Based on the developed prediction model, the effect of initial groove angle on strain rate inside and outside groove was investigated. Based on the evolution of strain rate, the corresponding normal stress and effective stress were also analyzed. Moreover, the established prediction model was verified by corresponding experimental FLCs of Ti6Al4V at 923 and 973 K with strain rate of 0.01 s^{-1} and 973 K with strain rate of 0.05 s^{-1}, which is widely used in the aerospace field [22,23].

2 Derivation of modified M−K model

The original M−K model assumes that the groove is perpendicular to the major principal stress direction, as shown in Fig. 1. However, the direction of original imperfection of sheet metal is random, as a result, a modified M−K model is proposed, which assumes that there is an initial groove angle ϕ_0 between the groove direction and the major principal stress direction, as shown in Fig. 2 [24]. Under each loading condition, the minimum value of the calculated forming limits is regarded as the forming limit when ϕ_0 varies from 0° to 90° [7]. Moreover, the strain increment along groove direction in Areas a and b is equal and the force normal to groove direction in Areas a and b is also equal. The elaborated stress analysis in Areas a and b is shown in Fig. 3.

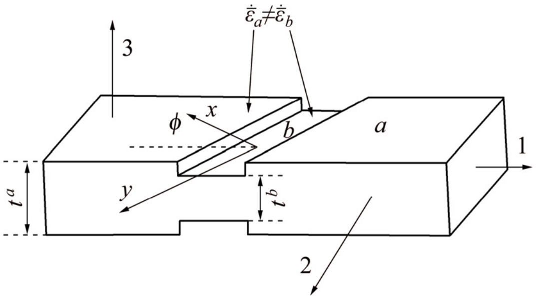

Fig. 2 Geometric diagram of modified M−K model [24]

Set $\alpha_{ijkl}=\sigma_{ij}/\sigma_{kl}$, and σ_{xx}^a, σ_{xy}^a, σ_{xx}^b and σ_{xy}^a are expressed as

$$\sigma_{xx}^a=\sigma_{11}^a(\alpha_{2211}^a\sin^2\phi+\cos^2\phi) \tag{1}$$

$$\sigma_{xy}^a=\sigma_{11}^a(\alpha_{2211}^a-1)\sin\phi\cos\phi \tag{2}$$

$$\sigma_{xx}^b=\sigma_{11}^b(\alpha_{2211}^b\sin^2\phi+\alpha_{1211}^b\sin2\phi+\cos^2\phi) \tag{3}$$

$$\sigma_{xy}^b=\sigma_{11}^b[\alpha_{1211}^b\cos2\phi+(\alpha_{2211}^b-1)\sin\phi\cos\phi] \tag{4}$$

where the subscripts x and y denote the normal and tangential directions of the groove, respectively; and the superscripts a and b denote Areas a and b, respectively [25].

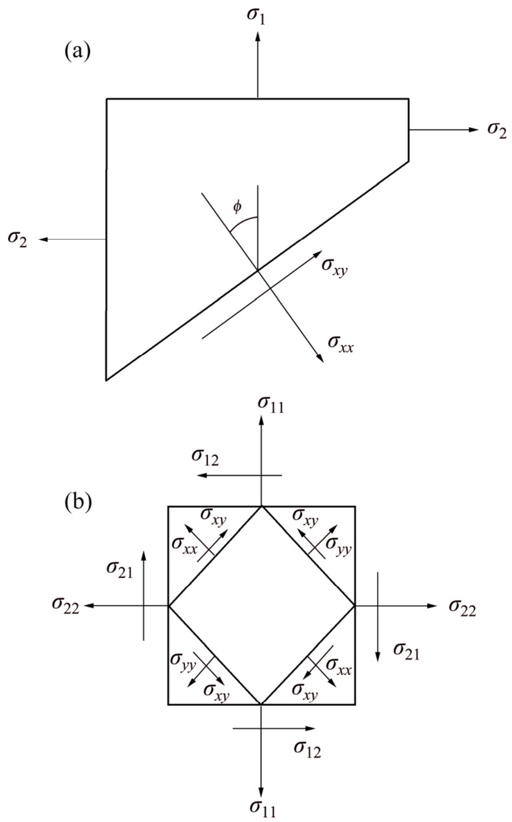

Fig. 3 Stress analysis diagrams for modified M−K model in different areas: (a) Area a; (b) Area b

There is a force equilibrium between Areas a and b, which can be expressed as

$$\begin{cases} F_{xy}^a=F_{xy}^b \\ F_{xx}^a=F_{xx}^b \end{cases} \tag{5}$$

Namely [26],

$$\begin{cases} \sigma_{xx}^a t_0^a\exp(\varepsilon_{33}^a)=\sigma_{xx}^b t_0^b\exp(\varepsilon_{33}^b) \\ \sigma_{xy}^a t_0^a\exp(\varepsilon_{33}^a)=\sigma_{xy}^b t_0^b\exp(\varepsilon_{33}^b) \end{cases} \tag{6}$$

where t_0^a and t_0^b denote the initial thicknesses of

Areas a and b, respectively, and ε_{33} is through-thickness strain. An initial thickness imperfection factor f is defined as $f=t_0^b/t_0^a$ [3,24].

From Eq. (6), we have

$$\frac{\sigma_{xx}^a}{\sigma_{xy}^a}=\frac{\sigma_{xx}^b}{\sigma_{xy}^b} \tag{7}$$

From Eqs. (1)−(7), it can be derived that

$$\frac{(\alpha_{2211}^b\sin^2\phi+\alpha_{1211}^b\sin 2\phi+\cos^2\phi)}{[\alpha_{1211}^b\cos 2\phi+(\alpha_{2211}^b-1)\sin\phi\cos\phi]}=\frac{(\alpha_{2211}^a\sin^2\phi+\cos^2\phi)}{(\alpha_{2211}^a-1)\sin\phi\cos\phi} \tag{8}$$

When a small principal strain increment $\mathrm{d}\varepsilon_{11}^a$ is imposed in Area a, the groove angle increment is set to be $\mathrm{d}\phi$, whose relation can be expressed as

$$\tan(\phi+\mathrm{d}\phi)=\frac{1+\mathrm{d}\varepsilon_{11}^a}{1+\mathrm{d}\varepsilon_{22}^a}\tan\phi \tag{9}$$

The relation of strain increments inside and outside groove is

$$\mathrm{d}\varepsilon_{yy}^a=\mathrm{d}\varepsilon_{yy}^b \tag{10}$$

Set $\rho_{ijkl}=\mathrm{d}\varepsilon_{ij}/\mathrm{d}\varepsilon_{kl}$, then

$$\mathrm{d}\varepsilon_{yy}^a=\mathrm{d}\varepsilon_{11}^a(\rho_{2211}^a\cos^2\phi+\sin^2\phi) \tag{11}$$

$$\mathrm{d}\varepsilon_{yy}^b=\mathrm{d}\varepsilon_{11}^b(\rho_{2211}^b\cos^2\phi+\sin^2\phi-2\rho_{1211}^b\sin\phi\cos\phi) \tag{12}$$

Generally, the instability occurs when $\mathrm{d}\bar{\varepsilon}^a/\mathrm{d}\bar{\varepsilon}^b$ is smaller than a critical value, while a smaller ratio value has no obvious influence on the level of FLC [27]. Hence, it is assumed in this study that when the ratio is smaller than 0.1 [26,28], the instability occurs.

The von Mises yield criterion is expressed as

$$Y(\sigma_{ij})=\sqrt{(\sigma_{11}-\sigma_{22})^2+\sigma_{22}^2+\sigma_{11}^2+6\sigma_{12}^2}\Big/\sqrt{2} \tag{13}$$

From Drucker postulate, we have

$$\mathrm{d}\varepsilon_{\mathrm{mn}}=\mathrm{d}\lambda\frac{\partial Y(\sigma_{ij})}{\partial\sigma_{mn}} \tag{14}$$

where $\mathrm{d}\lambda$ is the plastic factor.

Namely,

$$\mathrm{d}\varepsilon_{11}=\mathrm{d}\lambda\frac{1}{\sqrt{2}}\frac{2\sigma_{11}-\sigma_{22}}{\sqrt{2}Y(\sigma_{ij})} \tag{15}$$

$$\mathrm{d}\varepsilon_{22}=\mathrm{d}\lambda\frac{1}{\sqrt{2}}\frac{2\sigma_{22}-\sigma_{11}}{\sqrt{2}Y(\sigma_{ij})} \tag{16}$$

$$\mathrm{d}\varepsilon_{12}=\frac{\mathrm{d}\lambda}{2}\frac{1}{\sqrt{2}}\frac{6\sigma_{12}}{\sqrt{2}Y(\sigma_{ij})} \tag{17}$$

In addition, the hypothesis of incompressibility gives

$$\mathrm{d}\varepsilon_{11}+\mathrm{d}\varepsilon_{22}+\mathrm{d}\varepsilon_{33}=0 \tag{18}$$

During forming, the stress state is plane stress, and the corresponding equivalent plastic work principle is expressed as

$$\bar{\sigma}\mathrm{d}\bar{\varepsilon}=\sum_{i=1}^{2}\sum_{j=1}^{2}\sigma_{ij}\mathrm{d}\varepsilon_{ij} \tag{19}$$

Set $\varphi_{11}=\bar{\sigma}/\sigma_{11}$, $\beta_{11}=\mathrm{d}\bar{\varepsilon}/\mathrm{d}\varepsilon_{11}$. From Eqs. (13), (15), (16) and (19), we have

$$\varphi_{11}=\sqrt{(1+\alpha_{2211}^2-\alpha_{2211}+3\alpha_{1211}^2)} \tag{20}$$

$$\beta_{11}=(1+\alpha_{2211}\alpha_{2211})/\varphi_{11} \tag{21}$$

$$\varphi_{11}\beta_{11}=1+\alpha_{2211}\rho_{2211}+2\alpha_{1211}\rho_{1211} \tag{22}$$

According to Druckers postulate, the following equations can be derived:

$$\rho_{2211}=\frac{2\alpha_{2211}-1}{2-\alpha_{2211}} \tag{23}$$

$$\rho_{1211}=\frac{3\alpha_{1211}}{2-\alpha_{2211}} \tag{24}$$

Set $\rho_y^b=\mathrm{d}\varepsilon_{yy}^b/\mathrm{d}\bar{\varepsilon}^b$, one can have

$$\rho_y^b=\frac{\mathrm{d}\varepsilon_{11}^b(\rho_{2211}^b\cos^2\phi+\sin^2\phi-2\rho_{1211}^b\sin\phi\cos\phi)}{\mathrm{d}\bar{\varepsilon}^b}=\frac{\rho_{2211}^b\cos^2\phi+\sin^2\phi-2\rho_{1211}^b\sin\phi\cos\phi}{\beta_{11}^b} \tag{25}$$

Due to the existence of thickness imperfection, the strain rate relation between Areas a and b is expressed as follows

$$\dot{\bar{\varepsilon}}_b=\frac{\mathrm{d}\bar{\varepsilon}_b}{\mathrm{d}\bar{\varepsilon}_a}\dot{\bar{\varepsilon}}_a \tag{26}$$

The Grosman equation is adopted when calculating forming limit, which is expressed as follows [7,29]:

$$\bar{\sigma}=K\bar{\varepsilon}^n\dot{\bar{\varepsilon}}^m\exp(s\bar{\varepsilon}) \tag{27}$$

where K, n, m and s are strength coefficient, strain hardening exponent, strain rate sensitivity coefficient and softening coefficient, respectively.

Set $\alpha=\alpha_{2211}^a$, which represents different linear loading paths. α=0 represents uniaxial tension state, and α=1 represents biaxial tension state. During calculation, the stress state α and initial groove angle ϕ_0 are set, and concrete calculation process is shown in Fig. 4. Then, the calculation process is repeated by setting different ϕ_0 values and selects the minimum limit strain as forming limit.

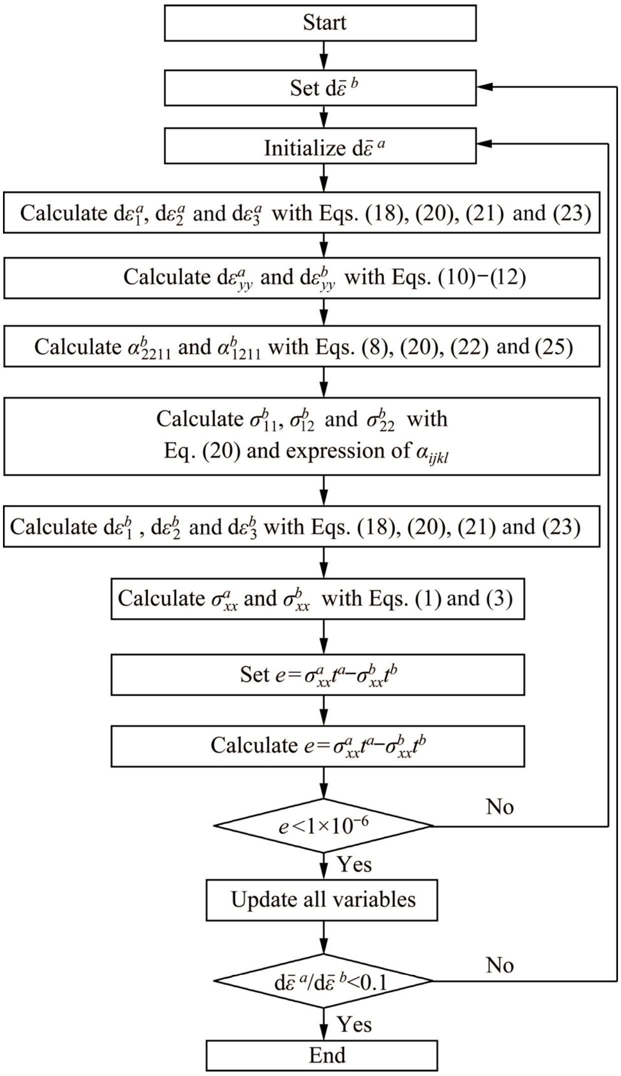

Fig. 4 Schematic showing calculation process of FLC

3 Result and discussion

3.1 Constitutive model

LI et al [12] carried out the uniaxial tension tests of Ti6Al4V at 923, 973 and 1023 K with strain rate range of 0.0005−0.05 s^{-1}. The corresponding data with strain smaller than 0.223 (fracture part) were selected for prediction in this study for convenient data processing and uniformity. It is essential to obtain a reliable constitutive model in order to obtain reasonable FLC prediction result. The true stress−true strain curves are transferred into plastic stress−strain curves by Eq. (28), which can also be used in finite element simulation directly.

$$\varepsilon^{\text{plastic}}=\varepsilon^{\text{true}}-\varepsilon^{\text{elastic}} \tag{28}$$

Taking logarithm on both sides of Eq. (27) gives the following relation:

$$\ln\bar{\sigma}=\ln K+n\ln\bar{\varepsilon}+m\ln\dot{\bar{\varepsilon}}+s\bar{\varepsilon} \tag{29}$$

Under given certain temperature and strain, the relation between $\ln\bar{\sigma}$ and $\ln\dot{\bar{\varepsilon}}$ is linear and the value of m can be obtained by linear fitting. Then the parameters K, n and s can be fitted through non-linear fitting method in MATLAB with Eq. (27) and the corresponding results are shown in Table 1. Fitted plastic stress−plastic strain curves are then transferred into true stress−true strain curves. The comparison between experimental and theoretical true stress−true strain curves is shown in Fig. 5. Compared with fitting result in Ref. [12], the fitting accuracy has been improved significantly. So, the Grosman equation used in this work is appropriate for FLC prediction. The temperature dependent variable m and the strain rate dependent variables K, n and s values can be obtained with linear interpolation between a number of parameters shown in Table 1.

3.2 Influence of initial groove angle on strain rate at different linear loading paths

It can be observed from Fig. 5 that strain hardening effect plays a dominant role at first, but high temperature softening effect becomes more and more important afterwards under the condition of 973 K with strain rate of 0.01 s^{-1}. At elevated temperature, high temperature softening effect makes it difficult to reach a force equilibrium between inside and outside groove and then results in the non-convergence of the algorithm. However, inhomogeneous thickness results in $\dot{\bar{\varepsilon}}_b>\dot{\bar{\varepsilon}}_a$, which makes the strain rate hardening effect in Area b be more obvious than that in Area a and makes the algorithm become convergent. To understand the effect of strain rate difference between inside and outside groove on the FLC prediction, it is necessary to investigate the variation of $\dot{\bar{\varepsilon}}_a$ and $\dot{\bar{\varepsilon}}_b$ during calculation.

Based on the FLC prediction of Ti6Al4V at 973 K with strain rate of 0.01 s^{-1}, the influence of ϕ_0 on strain rate ($\dot{\bar{\varepsilon}}_a$, $\dot{\bar{\varepsilon}}_b$) is investigated with the derived model in this work.

During calculation, the effective strain increment in Area b is constant, namely $d\bar{\varepsilon}^b\equiv$ 0.005, so it is reasonable to adopt the effective strain

Table 1 Fitted values of K, n, m and s under different conditions

Temperature/K	Strain rate/s^{-1}	K	n	m	s
923	0.0005	724.8	0.02088	0.115899	−1.168
	0.001	736.6	0.02367		−0.6234
	0.005	912.5	0.08461		−0.6249
	0.01	865.7	0.08371		−0.5832
	0.05	786.8	0.07735		−0.4979
973	0.0005	686.4	9.37×10^{-10}	0.166735	−1.131
	0.001	740.6	0.000163		−1.039
	0.005	807.4	0.03583		−0.7429
	0.01	789.5	0.03801		−0.5143
	0.05	762.3	0.06225		−0.5127
1023	0.0005	675.6	7.05×10^{-10}	0.2151309	−1.982
	0.001	723.3	5.33×10^{-5}		−1.567
	0.005	616.9	0.01472		−0.4463
	0.01	672.7	0.004941		−0.5969
	0.05	688.1	0.04941		−0.8043

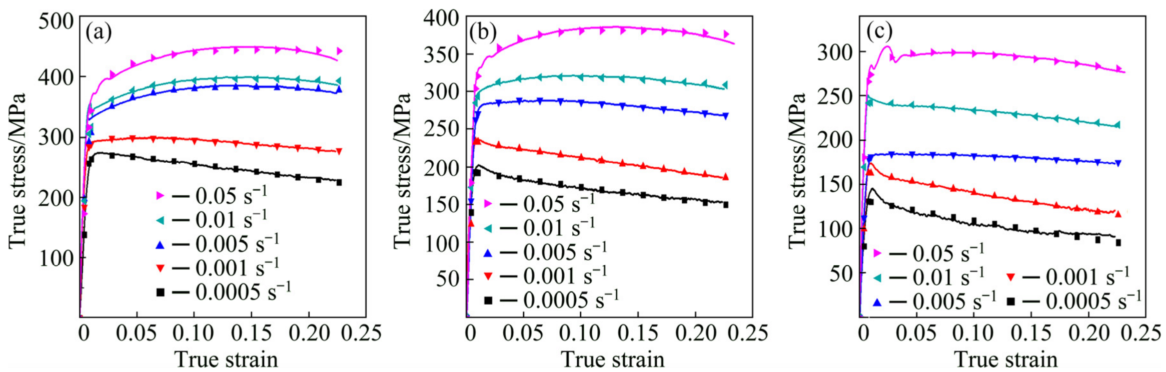

Fig. 5 Comparison between experimental (solid curves) [12] and theoretical (symbols) true stress−true strain curves at indicated strain rates and temperatures: (a) 923 K; (b) 973 K; (c) 1023 K

in Area b to represent the calculation process in this work. In the derived model, the effective strain rate of 0.01 s^{-1} is applied to Area a, which means $\dot{\bar{\varepsilon}}_a\equiv$ 0.01 s^{-1}. During calculation, when the sheet is formed at different linear loading paths, the corresponding effective strain rate in Area b with various ϕ_0 is shown in Fig. 6. It can be observed from Fig. 6 that when $0\le\alpha<0.5$, the calculated forming limit first decreases and then increases with increasing ϕ_0, which is the same as that in Ref. [30]. Moreover, ϕ_0 contributes a high effect on the evolution of effective strain rate during the calculation. When $0.5\le\alpha<1$, the calculated forming limit increases with the increase of ϕ_0. Moreover, when $0.5\le\alpha<1$, the effective strain rate curves with different ϕ_0 at a certain α become closer to each other with the increase of α, which means that ϕ_0 has a smaller effect on the evolution of effective strain rate when loading path changes from plain strain condition to equi-biaxial tension condition. Especially when α=1, the evolution curves of effective strain rate with different ϕ_0 (Fig. 6(g)) become coincident. Figure 7 demonstrates corresponding prediction results of forming limit at α=1 with different ϕ_0 values, which shows that ϕ_0 has no influence on the FLC prediction under equi-biaxial tension condition. This phenomenon can be explained by Eq. (23) and Eq. (9). From Eq. (23), it can be derived that when α=1, ρ_{2211}=1, which shows that $d\varepsilon_1^a=d\varepsilon_2^a$. From Eq. (9), it can be derived that $\tan(\phi+d\phi)=\tan\phi$, namely $d\phi=0$. In summary, with the increase of α, the influence of ϕ_0

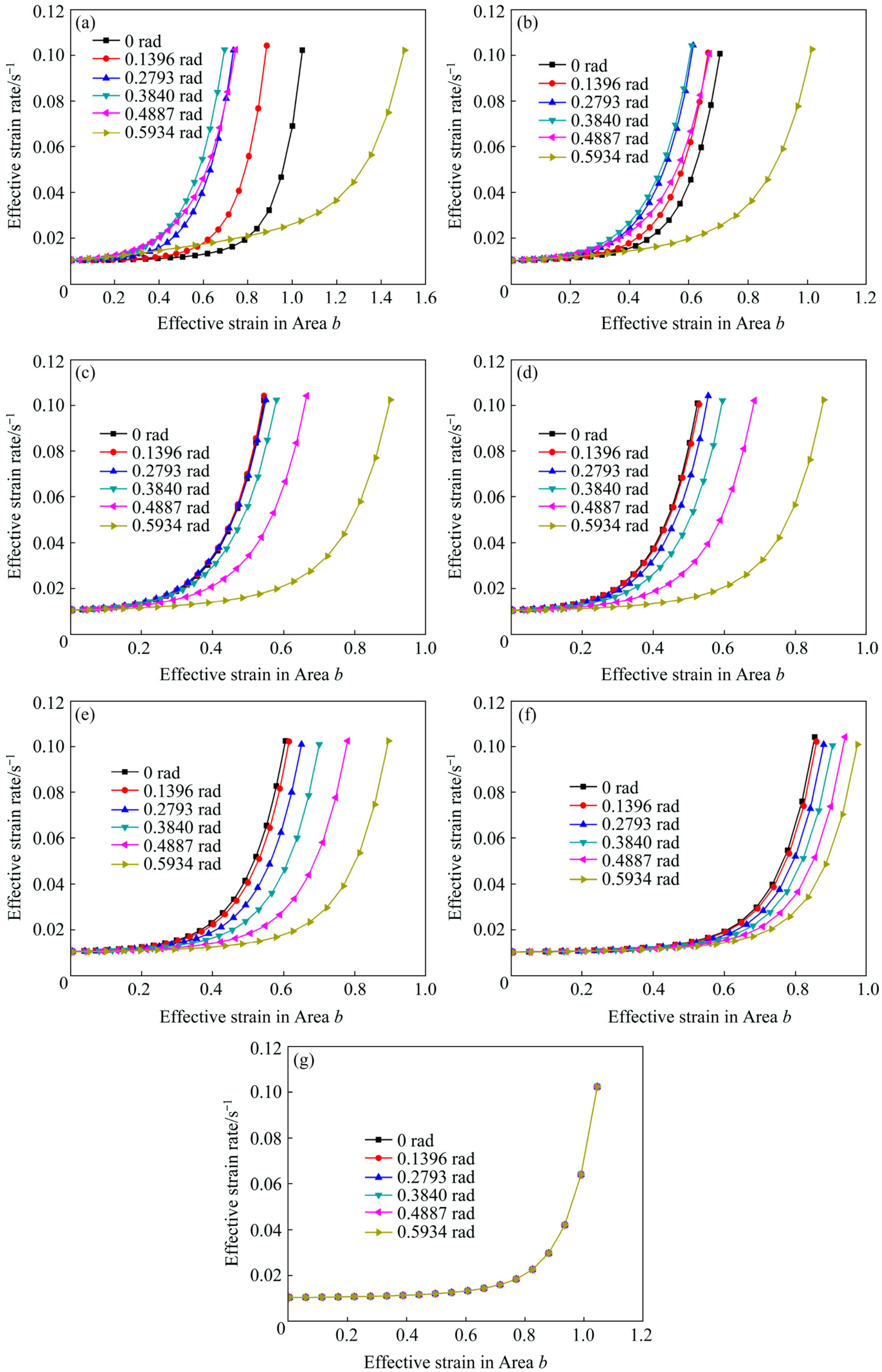

Fig. 6 Evolution curves of effective strain rate in Area *b* at different ϕ_0: (a) α=0; (b) α=0.2; (c) α=0.4; (d) α=0.5; (e) α=0.7; (f) α=0.9; (g) α=1

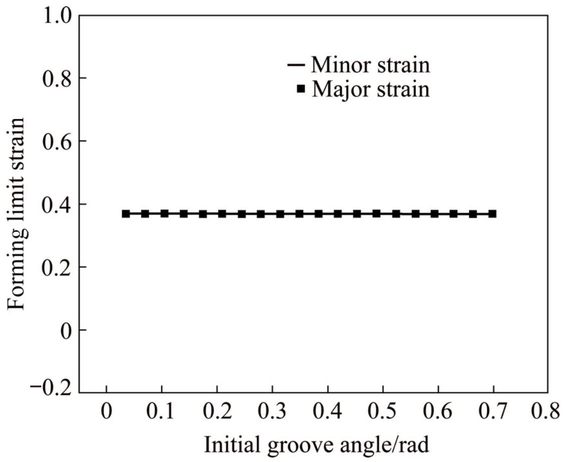

Fig. 7 Prediction results of forming limit stain at α=1 with different initial groove angles ϕ_0

on the evolution of effective strain rate becomes weaker. Moreover, when α=1, the groove angle remains constant and ϕ_0 has no effect on the FLC prediction.

In addition, Fig. 6 shows that the effective strain rate in Area b and the slope of effective strain rate curves in Area b increase during calculation due to the interaction of strain rate hardening effect and high temperature softening effect. The strain hardening effect plays a dominant role with small $\bar{\varepsilon}_b$ values (Fig. 5(b)). As calculation proceeds, high temperature softening effect is dominant with increasing $\bar{\varepsilon}_b$ values (Fig. 5(b)). However, the hardening effect in Area b needs to be more obvious than that in Area a in order to satisfy Eq. (5), and hardening effect can be improved by increasing strain rate, namely strain rate hardening effect, which results in the rapid increase of slope of effective strain rate. The convergence process of prediction algorithm is contributed by the interaction of strain hardening effect, high temperature softening effect and strain rate hardening effect for the FLC prediction at elevated temperature.

3.3 Influence of strain rate difference on stress evolution

In order to gain a good understanding of the effect of strain rate difference between inside and outside groove on the prediction of forming limit, it is necessary to study the stress variation in Areas a and b during calculation. ϕ_0=0.5934 rad is selected for calculation in this section and the corresponding evolution of stress σ_{xx}^a, σ_{xx}^b, $\bar{\sigma}^a$ and $\bar{\sigma}^b$ during calculation are shown in Fig. 8. It can be found that when $\bar{\varepsilon}_b$>0.08, the stress begins to decrease with

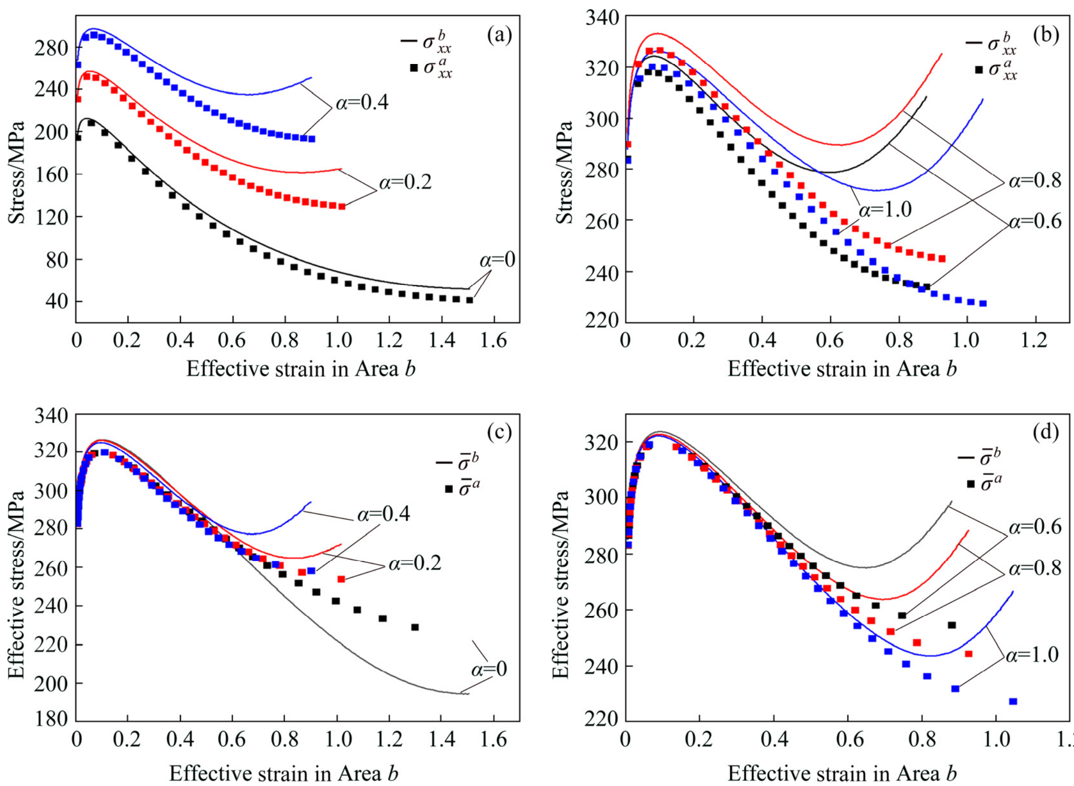

Fig. 8 Evolution of σ_{xx}^a, σ_{xx}^b, $\bar{\sigma}^a$ and $\bar{\sigma}^b$ during entire calculation when ϕ_0=0.5934 rad: (a) σ_{xx}^a and σ_{xx}^b with α=0−0.4; (b) σ_{xx}^a and σ_{xx}^b with α=0.6−1.0; (c) $\bar{\sigma}^a$ and $\bar{\sigma}^b$ with α=0−0.4; (d) $\bar{\sigma}^a$ and $\bar{\sigma}^b$ with α=0.6−1.0

the increase of strain, which is consistent with that in Fig. 5.

As shown in Fig. 8, σ_{xx}^{b} is higher than σ_{xx}^{a} during entire calculation, which is consistent with the fundamental of M−K theory. When 0.2≤α and $\bar{\varepsilon}_b$ < 0.8, the σ_{xx}^{b} and $\bar{\sigma}^{b}$ decrease with the increase of $\bar{\varepsilon}_b$. According to Eq. (9), frame xy is rotating during calculation and the groove angle become larger, which leads to the decrease of σ_{xx}^{b}. Meanwhile, high temperature softening effect also leads to the decrease of σ_{xx}^{b}. Therefore, the decrease of σ_{xx}^{b} is mainly due to the high temperature softening effect and the rotation of frame xy. When 0.2≤α and $\bar{\varepsilon}_b$>0.8, the σ_{xx}^{b} and $\bar{\sigma}^{b}$ begins to increase with the increase of $\bar{\varepsilon}_b$, which is mainly caused by rapid increase of $\dot{\bar{\varepsilon}}_b$. As shown in Fig. 6, when $\bar{\varepsilon}_b$ >0.8, $\dot{\bar{\varepsilon}}_b$ begins to increase rapidly, which makes the material in Area b become harder (due to the strain rate hardening effect) than that in Area a. In addition, the evolution of σ_{xx}^{b} and $\bar{\sigma}^{b}$ with α=0 is different from that with 0.2≤α<1. When α=0, the rotation rate of groove angle is larger than that when 0.2≤α<1, which leads to larger reduction of σ_{xx}^{b}. Moreover, for α=0, $\dot{\bar{\varepsilon}}_b$ starts to increase rapidly when $\bar{\varepsilon}_b$>1.3 (Fig. 6(a)), which makes the reduction rate of stress slow and the stress increase gradually. Hence, for the material with serious softening effect at elevated temperatures, the process of force equilibrium is the interaction of strain rate hardening effect and high temperature softening effect.

3.4 Verification of FLC prediction model at elevated temperatures

The FLCs of Ti6Al4V at 923 and 973 K with a strain rate of 0.01 s^{-1} from experimental work by BAI and WU [31] have been predicted by the derived M−K model and fitted Grosman equation in this study, and corresponding results are compared in Fig. 9(a) and Fig. 10(a). Both figures show a

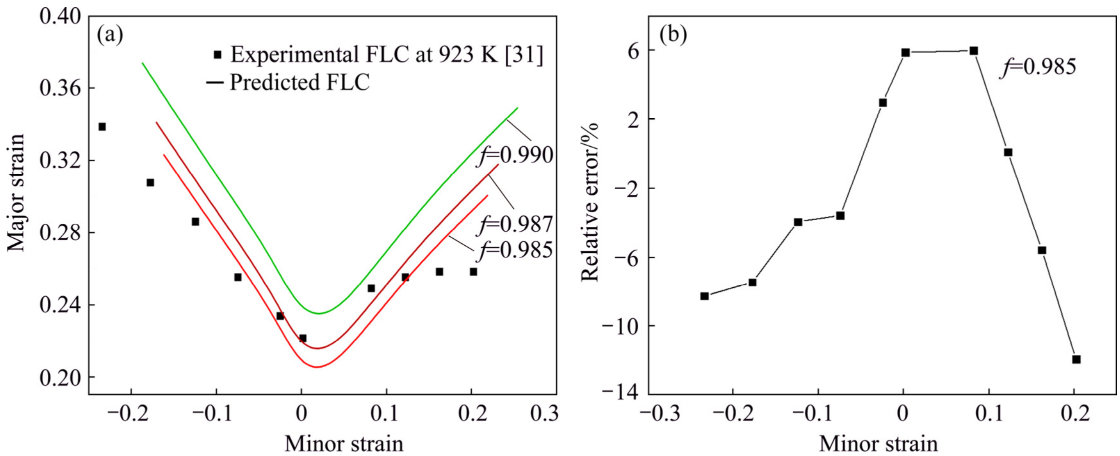

Fig. 9 Forming limit curves and relative error of Ti6Al4V at 923 K with strain rate of 0.01 s^{-1}: (a) Comparison between experimental and predicted FLC; (b) Distribution of relative error

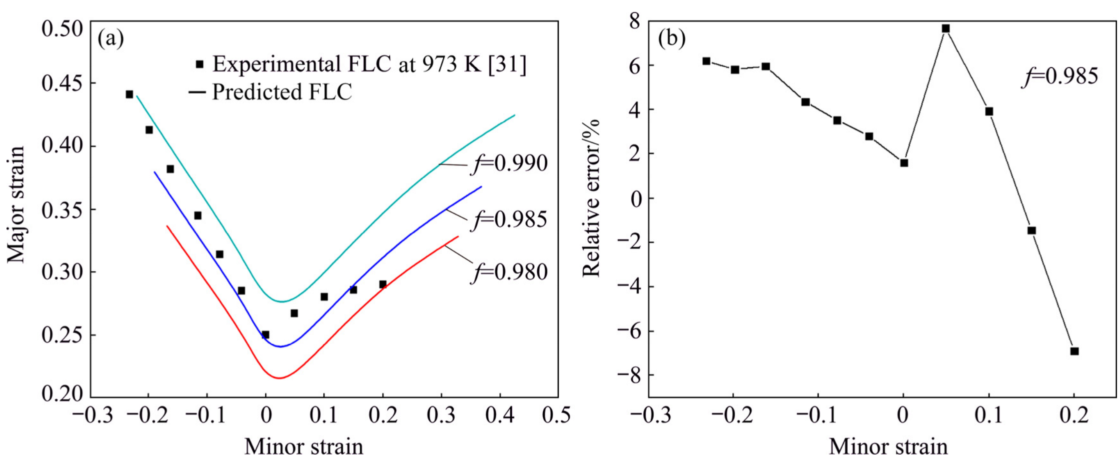

Fig. 10 Forming limit curves and relative error of Ti6Al4V at 973 K with strain rate of 0.01 s^{-1}: (a) Comparison between experimental and predicted FLC; (b) Distribution of relative error

good correspondence between the predicted FLCs and experimental results. However, it should be noted that when the effective strain is larger than 0.2, an apparent difference between the predicted FLCs and experimental results occurs. This is because the stress−strain curves beyond effective strain of 0.2 are extrapolated in this study, rather than those obtained from experiments.

In order to quantify the prediction accuracy of the developed FLC prediction model, the relative error is defined as Eq. (30) with the same minor strain.

$$\Delta=\frac{\varepsilon_{1\mathrm{p}}-\varepsilon_{1\mathrm{e}}}{\varepsilon_{1\mathrm{e}}}\times 100\% \tag{30}$$

where Δ is the relative error; $\varepsilon_{1\mathrm{p}}$ is the predicted value of FLC; $\varepsilon_{1\mathrm{e}}$ is the experimental value of FLC.

The distribution of relative error at 923 K with strain rate of 0.01 s^{-1} is shown in Fig. 9(b). The maximum relative error is about −12% when minor strain is about 0.2. However, the absolute value of relative error is less than 8% on the whole, indicating that the introduced method can predict the FLC of Ti6Al4V well at 923 K with strain rate of 0.01 s^{-1}.

Figure 10(b) shows the distribution of relative error at 973 K with strain rate of 0.01 s^{-1}. The maximum relative error is about 8%. However, the absolute value of relative error is less than 6% on the whole, which shows that the introduced method can predict the FLC of Ti6Al4V well at 973 K with strain rate of 0.01 s^{-1}.

In addition, the introduced method has also been applied to predicting FLCs of Ti6Al4V at 973 K with strain rate of 0.05 s^{-1} from Ref. [12]. For consistency, the adopted material parameters are the same as those in Ref. [12], and the predicted FLCs are compared with experimental results in Fig. 11(a). It can be observed that with the model introduced in this study, the prediction accuracy of FLC can be improved significantly, especially in negative minor strain region.

The distribution of relative error at 973 K with strain rate of 0.05 s^{-1} is shown in Fig. 11(b). The maximum absolute value of relative error is 11%. However, the absolute value of relative error is less than 8% on the whole, which shows that the introduced calculation method is also appropriate for predicting the FLC of Ti6Al4V at 973 K with strain rate of 0.05 s^{-1}.

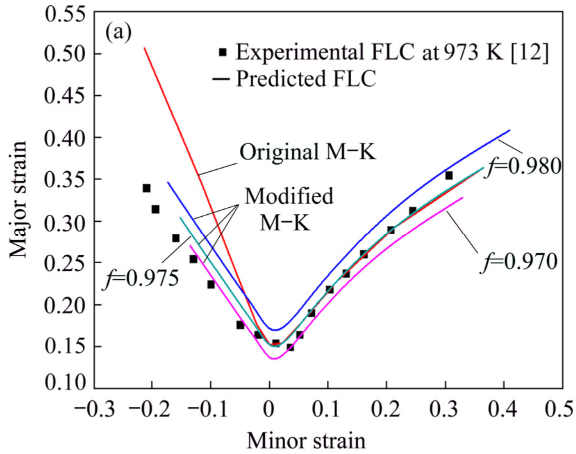

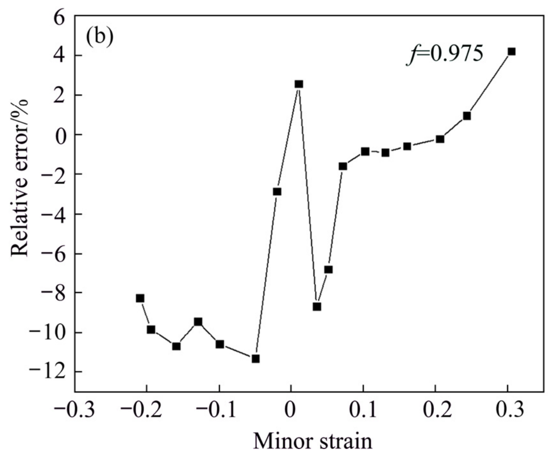

Fig. 11 Forming limit curves and relative error of Ti6Al4V at 973 K with strain rate of 0.05 s^{-1}: (a) Comparison between experimental and predicted FLC; (b) Distribution of relative error

4 Conclusions

(1) When the linear loading path changes from uniaxial tension to equi-biaxial tension, the influence of the initial groove angle on the evolution of strain rate becomes weaker in the M−K model.

(2) For the calculation of forming limit at elevated temperatures, the decrease of normal stress inside groove is mainly caused by the combined effect from high temperature softening effect and the rotation of groove, while the increase of normal stress inside groove is mainly caused by the strain rate hardening effect.

(3) The FLCs of Ti6Al4V at high temperatures and different strain rates can be fairly predicted by the established model, with which the absolute value of relative error is within 12%.

References

[1] KEELER S P, BACKOFEN W A. Plastic instability and fracture in sheets stretched over rigid punches [J]. ASM Transactions Quarterly, 1963, 56: 25−48.

[2] CHEN Jie-shi, ZHOU Xian-bin. A new curve fitting method for forming limit experimental data [J]. Journal of Materials Science & Technology, 2005, 21(4): 521−525.

[3] MARCINIAK Z, KUCZYŃSKI K. Limit strains in the processes of stretch-forming sheet metal [J]. International Journal of Mechanical Sciences, 1967, 9(9): 609−620.

[4] SAFDARIAN R. Stress based forming limit diagram for formability characterization of 6061 aluminum [J]. Transactions of Nonferrous Metals Society of China, 2016, 26(9): 2433−2441.

[5] WU Yong, LIU Gang, WANG Kai, LIU Zhi-qiang, YUAN Shi-jian. Loading path and microstructure study of Ti−3Al−2.5V tubular components within hot gas forming at 800 °C [J]. The International Journal of Advanced Manufacturing Technology, 2016, 87: 1823−1833.

[6] FAN Xiao-guang, YANG He, GAO Peng-fei. The mechanism of flow softening in subtransus hot working of two-phase titanium alloy with equiaxed structure [J]. Chinese Science Bulletin, 2014, 59(23): 2859−2867.

[7] WU Yong, LIU Gang, LIU Zhi-qiang, WANG Bin. Formability and microstructure of Ti22Al24.5Nb0.5Mo rolled sheet within hot gas bulging tests at constant equivalent strain rate [J]. Materials & Design, 2016, 108: 298−307.

[8] CAO Xiang-qing, XU Ping-ping, FAN Qi, WANG Wen-xian. Theoretical prediction of forming limit diagram of AZ31 magnesium alloy sheet at warm temperatures [J]. Transactions of Nonferrous Metals Society of China, 2016, 26(9): 2426−2432.

[9] ZHOU Jing, MU Yan-hong, WANG Bao-yu. A damage-coupled unified viscoplastic constitutive model for prediction of forming limits of 22MnB5 at high temperatures [J]. International Journal of Mechanical Sciences, 2017, 133: 457−468.

[10] HOU Bo, YU Zhong-qi, LI Shu-hui, LIN Zhong-qin. Prediction of forming limit diagram of aluminum sheet at elevated temperatures [J]. Materials Science & Technology, 2009, 17(5): 616−619.

[11] KOTKUNDE N, SRINIVASAN S, KRISHNA G, GUPTA A K, SINGH S K. Influence of material models on theoretical forming limit diagram prediction for Ti−6Al−4V alloy under warm condition [J]. Transactions of Nonferrous Metals Society of China, 2016, 26(3): 736−746.

[12] LI Xiao-qiang, GUO Gui-qiang, XIAO Jun-jie, SONG Nan, LI Dong-sheng. Constitutive modeling and the effects of strain rate and temperature on the formability of Ti−6Al−4V alloy sheet [J]. Materials & Design, 2014, 55(6): 325−334.

[13] MIRFALAH-NASIRI S M, BASTI A, HASHEMI R. Forming limit curves analysis of aluminum alloy considering the through-thickness normal stress, anisotropic yield functions and strain rate [J]. International Journal of Mechanical Sciences, 2016, 117: 93−101.

[14] SHAO Z T, BAI Q, LI N, LIN J, SHI Z, STANTON M, WATSON D, DEAN T A. Experimental investigation of forming limit curves and deformation features in warm forming of an aluminum alloy [J]. Journal of Engineering Manufacture, 2018, 232(3): 465−474.

[15] LI F F, FU M W, LIN J P, WANG X N. Experimental and theoretical study on the hot forming limit of 22MnB5 steel [J]. International Journal of Advanced Manufacturing Technology, 2014, 71: 297−306.

[16] NEIL C J, AGNEW S R. Crystal plasticity-based forming limit prediction for non-cubic metals: Application to Mg alloy AZ31B [J]. International Journal of Plasticity, 2009, 25(3): 379−398.

[17] CHAN L C, LU X Z. Material sensitivity and formability prediction of warm-forming magnesium alloy sheets with experimental verification [J]. International Journal of Advanced Manufacturing Technology, 2014, 71: 253−262.

[18] ZHENG Xing-yue, CHEN Jie-shi. The prediction and influence factors analysis of high temperature forming limit based on M−K theory [J]. Die & Mould Technology, 2017, 6: 1−6.

[19] GAO H X, FAKIR O E, WANG L L, POLITIS D J, LI Z Q. Forming limit prediction for hot stamping processes featuring non-isothermal and complex loading conditions [J]. International Journal of Mechanical Sciences, 2017, 131−132: 792−810.

[20] LIU Hong-wei, YAO Sheng-jie, LIU Wen-liang, ZHANG Zhao-duo. Forming limit diagram of magnesium alloy ZK60 at elevated temperature [J]. Advanced Materials Research, 2011, 308−310: 2442−2445.

[21] MA Bo-lin, WAN Min, WU Xiang-dong, CAI Zhao-yang, DIAO Ke-shan, HAN Jin-quan. Investigation on forming limit of advanced high strength steels (AHSS) under hot stamping conditions [J]. Journal of Manufacturing Processes, 2017, 30: 320−327.

[22] YANG He, FAN Xiao-guang, SUN Zhi-chao, GUO Liang-gang, ZHAN Mei. Recent developments in plastic forming technology of titanium alloys [J]. Science China: Technological Sciences, 2011, 54(2): 490−501.

[23] WANG Min, ZHOU Jian-xin, YIN Ya-jun, NAN Hai, XUE Peng-ju, TU Zhi-xin. Hot deformation behavior of the Ti6Al4V alloy prepared by powder hot isostatic pressing [J]. Journal of Alloys and Compounds, 2017, 721: 320−332.

[24] HUTCHINSON J W, NEALE K W. Mechanics of sheet metal forming [M]. New York: Plenum Press, 1978: 269−285.

[25] WANG Hai-bo, WAN Min. Forming limit of sheet metals based on mixed hardening model [J]. Science China: Technological Sciences, 2009, 52(5): 1202−1211.

[26] ASSEMPOUR A, NEJADKHAKI H K, HASHEMI R. Forming limit diagrams with the existence of through-thickness normal stress [J]. Computational Materials Science, 2010, 48(3): 504−508.

[27] DING Jie, ZHANG Chun-sheng, CHU Xing-rong, ZHAO Guo-qun, LEOTOING L, GUINESC D. Investigation of the influence of the initial groove angle in the M−K model on limit strains and forming limit curves [J]. International Journal of Mechanical Sciences, 2015, 98: 59−69.

[28] ZHANG Fei-fei, CHEN Jie-shi, CHEN Jun, ZHU Xin-hai. Forming limit model evaluation for anisotropic sheet metals under through-thickness normal stress [J]. International Journal of Mechanical Sciences, 2014, 89: 40−46.
[29] GRONOSTAJSKI Z. The constitutive equations for FEM analysis [J]. Journal of Materials Processing Technology, 2000, 106: 40−44.
[30] ABED-MERAIM F, BALAN T, ALTMEYER G. Investigation and comparative analysis of plastic instability criteria: Application to forming limit diagrams [J]. The International Journal of Advanced Manufacturing Technology, 2014, 71(5−8): 1247−1262.
[31] BAI Xue-piao, WU Xiang-dong. Forming limit diagram and its application for Ti−6Al−4V alloy sheet at elevated temperature [J]. Journal of Plasticity Engineering, 2013, 20(3): 102−105.

M−K 模型中凹槽内、外应变速率差对 Ti6Al4V 合金高温成形极限曲线预测的影响

李小强[1]，董红瑞[1]，王海波[2]，郭贵强[1]，李东升[1]

1. 北京航空航天大学 机械工程及自动化学院，北京 100191；
2. 北方工业大学 机械与材料工程学院，北京 100144

摘　要：研究初始凹槽角对 Ti6Al4V 合金凹槽内、外应变速率的影响。基于凹槽内、外应变速率的变化，分析应变速率差对凹槽内、外正应力和等效应力演变的影响。研究结果表明，在 M−K 模型中，当线性加载路径由单向拉伸变化到等双拉伸时，初始槽角对应变速率变化的影响减弱。由于凹槽内、外力平衡的约束，在计算过程中应变速率差使凹槽内的正应力先降低后升高，这使得合金高温下成形极限的预测算法收敛。凹槽内正应力的降低主要由高温软化效应和凹槽旋转引起，而凹槽内正应力的升高主要由应变速率硬化效应引起。

关键词：Ti6Al4V 合金；应变率速差；成形极限；M−K 模型；应力演变

(Edited by Wei-ping CHEN)